

# **Inverse modeling of hydrologic systems with adaptive multi-fidelity simulations**

Jiangjiang Zhang<sup>1</sup>, Jun Man<sup>1</sup>, Laosheng Wu<sup>2</sup>, and Lingzao Zeng<sup>1\*</sup>

<sup>1</sup> Zhejiang Provincial Key Laboratory of Agricultural Resources and Environment, Institute of Soil and Water Resources and Environmental Science, College of Environmental and Resource Sciences, Zhejiang University, Hangzhou, 310058, China,

<sup>2</sup> Department of Environmental Sciences, University of California Riverside, Riverside, CA, 92521, USA.

\* Correspondence to:

L. Zeng,  
[lingzao@zju.edu.cn](mailto:lingzao@zju.edu.cn)

# Abstract

Markov chain Monte Carlo (MCMC) simulation methods are widely used to assess parameter uncertainties of hydrologic models conditioned on measurements of observable state variables. However, when the model is CPU-intensive, the computational cost of MCMC simulation will be prohibitive. In this situation, an efficient while less accurate low-fidelity model (e.g., a numerical model with a coarser discretization, or a data-driven surrogate) is usually adopted. When integrating the high and low-fidelity models in a proper manner, we can balance both efficiency and accuracy in the MCMC simulation. As the posterior distribution of the unknown model parameters is the region of our interest, it is wise to distribute most of the computational budget therein. Based on this idea, we propose an adaptive multi-fidelity simulation-based MCMC algorithm for efficient inverse modeling of hydrologic systems in this paper. Here, we evaluate the high-fidelity model mainly in the posterior region through iteratively running MCMC based on a Gaussian process (GP) system adaptively constructed with multi-fidelity simulations. The error of the GP system is rigorously considered in the MCMC simulations and gradually reduced to a negligible level. Thus, the proposed method can obtain an accurate estimate of the posterior distribution with a very low computational cost, whose performance is demonstrated with two numerical case studies in inverse modeling of hydrologic systems.

## 1. Introduction

For better understanding and management of hydrologic systems, there is a growing interest in applying numerical modeling techniques to conduct qualitative and quantitative analyses [Anderson *et al.*, 2015; Vieux, 2001]. However, the existence of uncertainties in model structure, model parameters, initial and boundary conditions, measurement data, etc., would hinder the predictive accuracy of hydrologic modeling [Clark *et al.*, 2011; Refsgaard *et al.*, 2012; Wagener and Gupta, 2005]. To reduce the predictive uncertainty of the hydrologic system of concern, it is common practice to calibrate the system model against measurements of some state variables, e.g., hydraulic head, solute concentration, temperature and streamflow, through solving an inverse problem.

When handling uncertainties in hydrologic modeling, inverse methods based on Bayes' theorem are appropriate options as they can be formulated in a coherent and consistent manner [Stuart, 2010; Vrugt, 2016]. In the Bayesian framework, quantities of interest are modeled as random variables and their posterior distribution is proportional to their prior distribution times the likelihood. In most situations, closed-forms of the posterior distribution are non-existent, so that one has to resort to Monte Carlo simulation methods to obtain a numerical approximation. Over the past decades, Markov chain Monte Carlo (MCMC) methods have been widely used to assess uncertainties of hydrologic models conditioned on measurements of observable state variables [Smith and Marshall, 2008]. Examples of MCMC algorithms that draw particular attention include the DRAM algorithm [Haario *et al.*, 2006] and the DREAM

algorithm [Vrugt, 2016; Vrugt *et al.*, 2008], etc. However, MCMC has to sufficiently explore the variable space before it converges to the posterior distribution, which usually means a large number of model evaluations. When the hydrologic model is CPU-intensive, the computational cost of MCMC simulation will be prohibitive.

To alleviate the computational cost, one can use a CPU-efficient low-fidelity model (denoted by  $f_L(\mathbf{m})$ , where  $\mathbf{m}$  signifies the model parameters) of the original model (denoted by  $f_H(\mathbf{m})$ , i.e., the high-fidelity model) in the MCMC simulation. A low-fidelity model could be a data-driven surrogate based on interpolation or regression, a numerical model that considers fewer processes or has a lower numerical precision (e.g., with a coarser discretization) or is constructed by projecting high-dimensional variables onto their low-dimensional subspace, etc. [Asher *et al.*, 2015; Razavi *et al.*, 2012; Smith, 2014]. Inevitably, using  $f_L(\mathbf{m})$  alone in the MCMC simulation will introduce some bias. To correct this bias, one popular approach is to further evaluate  $f_H(\mathbf{m})$  in a two-stage manner [Efendiev *et al.*, 2005; Laloy *et al.*, 2013; Zeng *et al.*, 2012; Zhang *et al.*, 2015]. More recently, another approach that adaptively refine a data-driven surrogate over the posterior distribution is proposed, which has shown to be highly efficient [Gong and Duan, 2017; Zhang *et al.*, 2016].

In the above approaches, the correlation between  $f_H(\mathbf{m})$  and  $f_L(\mathbf{m})$  is not considered, which leaves some potential untouched. One method that is suitable for fusing  $f_H(\mathbf{m})$  and  $f_L(\mathbf{m})$  into an integrated model is the multi-fidelity simulation [Kennedy and O'hagan, 2000]. Given a small number of  $f_H(\mathbf{m})$  evaluations and a much larger number of  $f_L(\mathbf{m})$  evaluations, the multi-fidelity simulation can take

advantage of both the efficiency of  $f_L(\mathbf{m})$  and the accuracy of  $f_H(\mathbf{m})$ . The integrated model can be constructed with many methods, e.g., polynomial chaos expansion [Narayan *et al.*, 2014; Palar *et al.*, 2016; Zhu *et al.*, 2014] and Gaussian process (GP) [Kennedy and O'hagan, 2000; Le Gratiet and Garnier, 2014; Parussini *et al.*, 2017; Raissi *et al.*, 2017]. In this paper, GP is adopted to construct the integrated model for multi-fidelity simulation, as GP is very flexible and can provide the uncertainty level (variance) of the system output. In the GP framework, the correlation between  $f_H(\mathbf{m})$  and  $f_L(\mathbf{m})$  is rigorously considered with the covariance functions and the corresponding hyperparameters are estimated with an optimization method conditioned on simulation data of both  $f_H(\mathbf{m})$  and  $f_L(\mathbf{m})$ .

In many cases, the posterior occupies a very small proportion of the prior region. If the multi-fidelity system is built over the whole prior distribution, its accuracy cannot be guaranteed as we can only afford a limited number of  $f_H(\mathbf{m})$  evaluations. Considering that the posterior distribution is the region of our interest, it is wise to distribute most of the computational budget (i.e.,  $f_H(\mathbf{m})$  evaluations) therein. Based on this idea, we propose an adaptive multi-fidelity simulation-based MCMC (AMF-MCMC) algorithm for efficient inverse modeling of hydrologic systems. Here, we iteratively run MCMC with a GP system constructed with multi-fidelity simulations to search the posterior region and accordingly add new  $f_H(\mathbf{m})$  evaluations to refine the GP system. Gradually, the GP system will be very accurate in the posterior region, based on which we can obtain an accurate estimate of the posterior distribution. In the AMF-MCMC algorithm, most of the  $f_H(\mathbf{m})$  simulations are applied near or within the

posterior region, thus very little computational budget is wasted.

The remainder of this paper is organized as follows. In Section 2, we provide detailed formulation of the AMF-MCMC algorithm. Then its performance is demonstrated with two numerical case studies in Section 3. Finally, some conclusions and discussions are provided in Section 4.

## 2. Methods

### 2.1. Bayesian inference with DREAM<sub>(zs)</sub>

For simplicity, here we represent the observation process of the hydrologic system of concern in the following compact form:

$$\mathbf{d} = f(\mathbf{m}) + \boldsymbol{\epsilon}, \quad (1)$$

where  $\mathbf{d}$  is a  $N_d$ -vector for the measurements,  $f(\cdot)$  is the system model,  $\mathbf{m}$  is a  $N_m$ -vector for the unknown model parameters, and  $\boldsymbol{\epsilon}$  is  $N_d$ -vector for the measurement errors. Before obtaining the measurements  $\mathbf{d}$ , our knowledge about the unknown model parameters  $\mathbf{m}$  is represented by the prior distribution,  $p(\mathbf{m})$ . When  $\mathbf{d}$  is available, we can update our knowledge about  $\mathbf{m}$  with the posterior distribution,  $p(\mathbf{m}|\mathbf{d})$ , according to Bayes' theorem:

$$p(\mathbf{m}|\mathbf{d}) = \frac{p(\mathbf{m})p(\mathbf{d}|\mathbf{m})}{p(\mathbf{d})}, \quad (2)$$

where  $L(\mathbf{m}|\mathbf{d}) \equiv p(\mathbf{d}|\mathbf{m})$  is the likelihood function that quantifies the mismatch between the model outputs  $f(\mathbf{m})$  and the measurements  $\mathbf{d}$ ,  $p(\mathbf{d}) = \int p(\mathbf{d}|\mathbf{m}) p(\mathbf{m}) d\mathbf{m}$  is the evidence.

In most situations, analytical forms of  $p(\mathbf{m}|\mathbf{d})$  does not exist. Here we resort to an efficient MCMC algorithm, i.e., DREAM<sub>(zs)</sub> (DiffeRential Evolution Adaptive

Metropolis [Vrugt, 2016; Vrugt *et al.*, 2008; Vrugt *et al.*, 2009]), to explore the parameter space and estimate  $p(\mathbf{m}|\mathbf{d})$  numerically. MCMC works by constructing a Markov chain that gradually converges to the posterior distribution. To better explore the parameter space,  $N_c$  parallel chains are generated and evolved simultaneously by DREAM<sub>(ZS)</sub>. At iteration  $t$ , DREAM<sub>(ZS)</sub> will propose a candidate state  $\mathbf{m}_p^i$  for the  $i$ th ( $i = 1, \dots, N_c$ ) chain with a mix of parallel direction jump (z) and snooker jump (s) based on an archive of thinned chain history,  $\mathbf{Z}$ , which is a  $N_m \times N_Z$  matrix. The parallel direction jump updates the previous state in the  $i$ th chain (i.e.,  $\mathbf{m}_{t-1}^i$ ) as follows:

$$\begin{aligned}\Delta\mathbf{m}_A^i &= \zeta_{d^*} + (1_{d^*} + \lambda_{d^*})\gamma_{(\delta, d^*)} \sum_{j=1}^{\delta} \left( \mathbf{Z}_A^{\mathbf{a}_j} - \mathbf{Z}_A^{\mathbf{b}_j} \right), \\ \Delta\mathbf{m}_{\neq A}^i &= 0,\end{aligned}\quad (3)$$

where  $\mathbf{m}_p^i = \mathbf{m}_{t-1}^i + \Delta\mathbf{m}^i$ ;  $A$  is a  $d^*$ -dimensional subspace of the  $N_m$ -dimensional parameter space;  $\zeta_{d^*}$  is a random sample drawn from a multivariate Gaussian distribution,  $\mathcal{N}_{d^*}(0, e_1)$ ;  $\lambda_{d^*}$  is a random sample drawn from a multivariate uniform distribution,  $\mathcal{U}_{d^*}(-e_2, e_2)$ . The default values for  $e_1$  and  $e_2$  are  $10^{-12}$  and 0.05, respectively;  $\gamma = 2.38/\sqrt{2\delta d^*}$  is the jump rate;  $\mathbf{a}$  and  $\mathbf{b}$  are  $\delta$  integers drawn from  $\{1, \dots, N_Z\}$  without replacement. The snooker jump generates  $\Delta\mathbf{m}^i$  in the following way:

$$\Delta\mathbf{m}^i = \zeta_{N_m} + \gamma_s (\mathbf{Z}_{\perp}^b - \mathbf{Z}_{\perp}^c), \quad (4)$$

where  $\zeta_{N_m} \sim \mathcal{N}_{N_m}(0, e_1)$ ;  $\gamma_s \sim \mathcal{U}(1.2, 2.2)$  is the snooker jump rate;  $\mathbf{Z}_{\perp}^b$  and  $\mathbf{Z}_{\perp}^c$  are projections of  $\mathbf{Z}^b$  and  $\mathbf{Z}^c$  onto the direction from  $\mathbf{m}_{t-1}^i$  to  $\mathbf{Z}^a$ , respectively;  $a, b$  and  $c$  are integers drawn from  $\{1, \dots, N_Z\}$  without replacement. In DREAM<sub>(ZS)</sub>,

the probabilities of using the parallel direction jump and the snooker jump are  $p_Z$  and  $p_S$ , where  $p_Z \geq 0$ ,  $p_S \geq 0$ , and  $p_Z + p_S = 1$ . Then we will compare the acceptance rate,  $p_{\text{acc}} = \min[1, p(\mathbf{m}_p^i | \mathbf{d})/p(\mathbf{m}_{t-1}^i | \mathbf{d})]$  with a random sample  $u$  drawn from  $\mathcal{U}(0,1)$ . If  $p_{\text{acc}} > u$ , we will accept  $\mathbf{m}_p^i$  and let  $\mathbf{m}_t^i = \mathbf{m}_p^i$ ; Otherwise, we will reject  $\mathbf{m}_p^i$  and let  $\mathbf{m}_t^i = \mathbf{m}_{t-1}^i$ . Every  $T_{\text{thin}}$  iterations, we will append the current  $N_c$  states in the Markov chains to the archive  $\mathbf{Z}$ . When the Markov chains converge to the stationary regime, we can view states in the chains as random samples drawn from the posterior distribution. For more details about DREAM<sub>(zs)</sub>, one can refer to [Vrugt, 2016].

## 2.2. Multi-fidelity simulation with Gaussian process

Before convergence, MCMC needs to sufficiently explore the parameter space, which generally requires a large number of model evaluations. When  $f(\mathbf{m})$  is CPU-intensive (then  $f(\mathbf{m})$  is called the high-fidelity model and represented by  $f_H(\mathbf{m})$  thereafter), the computational cost of MCMC simulation will be prohibitive. In this situation, a CPU-efficient low-fidelity model  $f_L(\mathbf{m})$  is usually adopted. To balance accuracy and efficiency, it is desirable to construct an integrated system for the MCMC simulation through fusing the information provided by a small number of  $f_H(\mathbf{m})$  evaluations and a much larger number of  $f_L(\mathbf{m})$  evaluations. This can be realized with the auto-regressive model [Kennedy and O'hagan, 2000]:

$$u_H(\mathbf{m}) = \rho u_L(\mathbf{m}) + \delta(\mathbf{m}), \quad (5)$$

where  $u_L(\mathbf{m}) \sim \mathcal{GP}(0, k_1(\mathbf{m}, \mathbf{m}'; \boldsymbol{\theta}_1))$  and  $\delta(\mathbf{m}) \sim \mathcal{GP}(0, k_2(\mathbf{m}, \mathbf{m}'; \boldsymbol{\theta}_2))$  are two independent GPs;  $k_i(\mathbf{m}, \mathbf{m}'; \boldsymbol{\theta}_i)$  are the covariance functions with hyperparameters

$\boldsymbol{\theta}_i$ ,  $i = 1, 2$ ;  $\rho$  is the cross-correlation coefficient. According to the property of Gaussian stochastic process,  $u_H(\mathbf{m})$  is also a GP [Raissi *et al.*, 2017]:

$$u_H(\mathbf{m}) \sim \mathcal{GP}(0, k(\mathbf{m}, \mathbf{m}'; \boldsymbol{\theta})), \quad (6)$$

where  $k(\mathbf{m}, \mathbf{m}'; \boldsymbol{\theta}) = \rho^2 k_1(\mathbf{m}, \mathbf{m}'; \boldsymbol{\theta}_1) + k_2(\mathbf{m}, \mathbf{m}'; \boldsymbol{\theta}_2)$ , and  $\boldsymbol{\theta} = [\boldsymbol{\theta}_1, \boldsymbol{\theta}_2, \rho]$ .

Consequently, we have:

$$\begin{bmatrix} u_L(\mathbf{m}) \\ u_H(\mathbf{m}) \end{bmatrix} \sim \mathcal{GP}\left(0, \begin{bmatrix} k_{LL} & k_{LH} \\ k_{HL} & k_{HH} \end{bmatrix}\right), \quad (7)$$

where  $k_{LL} = k_1(\mathbf{m}, \mathbf{m}'; \boldsymbol{\theta}_1)$ ,  $k_{LH} = k_{HL}^T = \rho k_1(\mathbf{m}, \mathbf{m}'; \boldsymbol{\theta}_1)$ , and  $k_{HH} = k(\mathbf{m}, \mathbf{m}'; \boldsymbol{\theta})$ . In this paper, we adopt the commonly used squared exponential covariance function [Williams and Rasmussen, 2006] for both  $k_1$  and  $k_2$ :

$$k_i(\mathbf{m}, \mathbf{m}'; \boldsymbol{\theta}_i) = \sigma_i^2 \exp\left[-\frac{1}{2} \sum_{n=1}^{N_m} \frac{(\mathbf{m}_n - \mathbf{m}'_n)^2}{\theta_{n,i}^2}\right], \quad (8)$$

where  $\boldsymbol{\theta}_i = [\sigma_i^2, (\theta_{n,i}^2)_{n=1}^{N_m}]$  are the hyperparameters of the covariance functions  $k_i$ , for  $i = 1, 2$ .

When data of  $N_L$  low-fidelity model evaluations and  $N_H$  high-fidelity model evaluations are available, we can estimate the hyperparameters by minimizing the negative log marginal likelihood:

$$NL = \frac{1}{2} \mathbf{D}^T \mathbf{K}^{-1} \mathbf{D} + \frac{1}{2} \log|\mathbf{K}| + \frac{N_L + N_H}{2} \log(2\pi), \quad (9)$$

where

$$\mathbf{K} = \begin{bmatrix} k_{LL}(\mathbf{M}_L, \mathbf{M}_L) + \sigma_L^2 \mathbf{I}_{N_L} & k_{LH}(\mathbf{M}_L, \mathbf{M}_H) \\ k_{HL}(\mathbf{M}_H, \mathbf{M}_L) & k_{HH}(\mathbf{M}_H, \mathbf{M}_H) + \sigma_H^2 \mathbf{I}_{N_H} \end{bmatrix}; \quad (10)$$

$\mathbf{M}_L = [\mathbf{m}_1, \dots, \mathbf{m}_{N_L}]$  are the  $N_L$  parameter samples for  $f_L(\mathbf{m})$ ,  $\mathbf{D}_L = [f_L(\mathbf{m}_1), \dots, f_L(\mathbf{m}_{N_L})]$  are the corresponding low-fidelity model outputs;  $\mathbf{M}_H =$

$[\mathbf{m}_1, \dots, \mathbf{m}_{N_H}]$  are the  $N_H$  parameter samples for  $f_H(\mathbf{m})$ ,  $\mathbf{D}_H = [f_H(\mathbf{m}_1), \dots, f_H(\mathbf{m}_{N_H})]$  are the corresponding high-fidelity model outputs;  $\mathbf{D} = [\mathbf{D}_L, \mathbf{D}_H]$ ;  $\mathbf{I}_{N_L}$  and  $\mathbf{I}_{N_H}$  are identify matrices of size  $N_L$  and  $N_H$ , respectively. Here, the hyperparameters to be estimated are  $[\boldsymbol{\theta}, \sigma_L^2, \sigma_H^2]$ .

After training the GP system conditioned on the multi-fidelity data  $\mathbf{D}$ , we can obtained a new GP system represented by  $\tilde{g}(\mathbf{m})$ , which can be used to predict the model output given an arbitrary parameter set  $\mathbf{m}^*$ :

$$\tilde{g}(\mathbf{m}^*) = u_H(\mathbf{m}^*) | \mathbf{D} \sim \mathcal{N}(\mu, \sigma^2), \quad (11)$$

where  $\mu = \mathbf{a}\mathbf{K}^{-1}\mathbf{D}$  is the mean estimate,  $\sigma^2 = k_{HH}(\mathbf{m}^*, \mathbf{m}^*) - \mathbf{a}\mathbf{K}^{-1}\mathbf{a}^T$  is the estimation variance, and  $\mathbf{a} = [k_{HL}(\mathbf{m}^*, \mathbf{M}_L) \ k_{HH}(\mathbf{m}^*, \mathbf{M}_H)]$ .

Then the multi-fidelity system  $\tilde{g}(\mathbf{m})$  can be used in MCMC simulations to gain efficiency. For more details about GP and its construction with multi-fidelity data, one can refer to [Kennedy and O'hagan, 2000; Parussini *et al.*, 2017; Raissi *et al.*, 2017; Williams and Rasmussen, 2006].

### 2.3. The adaptive multi-fidelity simulation-based MCMC algorithm

Generally, we can only afford a limited number of  $f_H(\mathbf{m})$  evaluations. If the multi-fidelity system  $\tilde{g}(\mathbf{m})$  is constructed over the whole prior distribution, its accuracy cannot be guaranteed. In MCMC simulation, our concern is the posterior distribution. Thus, we have to make sure that  $\tilde{g}(\mathbf{m})$  is accurate enough therein but there is no need to ensure its accuracy everywhere. Below we propose an adaptive multi-fidelity simulation-based MCMC (AMF-MCMC) algorithm which adaptively refines  $\tilde{g}(\mathbf{m})$  over the posterior distribution and finally obtains an accurate estimate

of  $p(\mathbf{m}|\mathbf{d})$ .

The AMF-MCMC algorithm first builds an initial multi-fidelity system  $\tilde{g}_0(\mathbf{m})$  conditioned on  $N_L$  evaluations of  $f_L(\mathbf{m})$  and  $N_H$  evaluations of  $f_H(\mathbf{m})$ , where  $N_H$  is a small integer and  $N_L$  is a number that is much larger than  $N_H$ . With  $\tilde{g}_0(\mathbf{m})$ , we can run DREAM<sub>(ZS)</sub> to sufficiently explore the parameter space, which can be done very quickly. Here, the variance of the GP system ( $\sigma_{\text{gp}}^2$ ) is considered in the MCMC simulation by augmenting it with the variance of the measurement error ( $\sigma_{\text{meas}}^2$ ), i.e.,  $\sigma_{\text{total}}^2 = \sigma_{\text{gp}}^2 + \sigma_{\text{meas}}^2$ , and using  $\sigma_{\text{total}}^2$  in the likelihood function,  $L(\mathbf{m}|\mathbf{d})$ . Then we can draw a random sample,  $\mathbf{m}_{\text{ap}}$ , from the approximated posterior,  $\tilde{p}_0(\mathbf{m}|\mathbf{d})$ , which is expected to be much closer to the posterior region than the prior samples. By utilizing the new data  $f_H(\mathbf{m}_{\text{ap}})$ , the multi-fidelity GP system can be refined locally. This process will be further repeated  $I_{\text{max}} - 1$  times. Finally, we can obtain a GP system that is locally very accurate in the posterior region and a very accurate estimate of  $p(\mathbf{m}|\mathbf{d})$ .

When implementing the AMF-MCMC algorithm, we can also collect more than one samples from the approximated posterior at each iteration, which can improve the simulation efficiency when  $f_L(\mathbf{m})$  is moderately CPU-intensive or  $f_L(\mathbf{m})$  can be evaluated in parallel. After each DREAM<sub>(ZS)</sub> simulation, the thinned chain history  $\mathbf{Z}$  will be saved and used in the next DREAM<sub>(ZS)</sub> simulation. Actually, this treatment tailors the  $I_{\text{max}} + 1$  MCMC simulations into an integrated one that has very long chains, which is beneficial to better explore the parameter space. The complete scheme of the AMF-MCMC algorithm is given in Algorithm 1.

---

**Algorithm 1** The adaptive multi-fidelity simulation-based MCMC algorithm.

---

1. Draw  $N_L$  random samples from the prior distribution,  $\mathbf{M}_L = [\mathbf{m}_1, \dots, \mathbf{m}_{N_L}]$ , calculate  $\mathbf{D}_L = [f_L(\mathbf{m}_1), \dots, f_L(\mathbf{m}_{N_L})]$ .
2. Draw  $N_H$  random samples from the prior distribution,  $\mathbf{M}_H = [\mathbf{m}_1, \dots, \mathbf{m}_{N_H}]$ , calculate  $\mathbf{D}_H = [f_H(\mathbf{m}_1), \dots, f_H(\mathbf{m}_{N_H})]$ . Here  $N_H \ll N_L$ .
3. Build the initial GP system  $\tilde{g}_0(\mathbf{m})$  with multi-fidelity simulation conditioned on  $[\mathbf{M}_L \mathbf{M}_H]$  and  $[\mathbf{D}_L \mathbf{D}_H]$ .
4. Run MCMC based on  $\tilde{g}_0(\mathbf{m})$ , obtain  $\tilde{p}_0(\mathbf{m}|\mathbf{d})$ .
5. **for**  $i = 1, \dots, I_{\max}$  **do**  
    Draw a random sample  $\mathbf{m}_{ap}$  from  $\tilde{p}_{i-1}(\mathbf{m}|\mathbf{d})$ , let  $\mathbf{M}_H = [\mathbf{M}_H \mathbf{m}_{ap}]$ ,  $\mathbf{D}_H = [\mathbf{D}_H f_H(\mathbf{m}_{ap})]$ .  
    Build the GP system  $\tilde{g}_i(\mathbf{m})$  conditioned on  $[\mathbf{M}_L \mathbf{M}_H]$  and  $[\mathbf{D}_L \mathbf{D}_H]$ .  
    Run MCMC based on  $\tilde{g}_i(\mathbf{m})$  and previous MCMC simulation results, obtain  $\tilde{p}_i(\mathbf{m}|\mathbf{d})$ .  
**end for**
6. The posterior  $p(\mathbf{m}|\mathbf{d})$  is approximated with  $\tilde{p}_{I_{\max}}(\mathbf{m}|\mathbf{d})$ .

---

### 3. Illustrative examples

#### 3.1. Example 1: Estimation of soil hydraulic and thermal parameters

In example 1, we first test the performance of the AMF-MCMC algorithm in estimating soil hydraulic and thermal parameters in a single ring infiltration experiment [Nakhaei and Šimůnek, 2014]. Here the processes of water flow and heat transport are considered. As shown in Figure 1, the flow domain is 100cm  $\times$  200cm. The initial conditions for water content and temperature in the domain are 0.1 and 17.5°C, respectively. The domain has three types of boundary conditions, i.e., impervious condition at the two lateral boundaries and part of the upper boundary (represented by the green lines), free drainage condition at the lower boundary (represented by the blue line) and constant temperature (61°C) and water content (0.43) conditions at part of the upper boundary (represented by the red line).

[Figure 1]

With the initial and boundary conditions prescribed above, we can simulate

unsaturated water flow in the domain by numerically solving the Richards' equation with HYDRUS-2D [*Šimůnek et al.*, 2008]:

$$\frac{\partial \theta}{\partial t} = \frac{\partial}{\partial x} \left[ K(h) \frac{\partial h}{\partial x} \right] + \frac{\partial}{\partial z} \left[ K(h) \frac{\partial h}{\partial z} + K(h) \right], \quad (12)$$

where  $\theta[-]$  is volumetric water content of the soil;  $t[\text{T}]$  is time;  $x[\text{L}]$  and  $z[\text{L}]$  are distances along the horizontal and vertical directions;  $h[\text{L}]$  is pressure head;  $K(h)[\text{LT}^{-1}]$  is hydraulic conductivity, which is a function of the pressure head  $h$  [Mualem, 1976; Vangenuchten, 1980]:

$$K(h) = K_s S_e^l \left[ 1 - (1 - S_e^{1/m})^m \right]^2, \quad (13)$$

where  $K_s[\text{LT}^{-1}]$  is saturated hydraulic conductivity,  $S_e[-]$  is effective saturation:

$$S_e = \frac{\theta - \theta_r}{\theta_s - \theta_r} = \begin{cases} \frac{1}{(1 + |\alpha h|^n)^m} & h < 0 \\ 1 & h \geq 0 \end{cases}, \quad (14)$$

where  $\theta_r$  and  $\theta_s$  are residual and saturated water content [-];  $l[-]$  is a pore-connectivity parameter;  $\alpha[\text{L}^{-1}]$ ,  $n[-]$  and  $m = (1 - 1/n)[-]$  are empirical shape parameters, respectively.

Based on the simulation of unsaturated water flow, we can further simulate the process of heat transport by numerically solving the following governing equation [*Sophocleous*, 1979] with HYDRUS-2D:

$$C(\theta) \frac{\partial T}{\partial t} = \frac{\partial}{\partial z} \left[ \lambda_{xz}(\theta) \frac{\partial T}{\partial x} \right] - C_w q_z \frac{\partial T}{\partial z}, \quad (15)$$

where  $C(\theta) = C_n \theta_n + C_o \theta_o + C_w \theta$  is volumetric heat capacity of soil [ $\text{ML}^{-1}\text{T}^{-2}\text{K}^{-1}$ ],  $C_n$ ,  $C_o$  and  $C_w$  are volumetric heat capacities of solid phase, organic phase and liquid phase [ $\text{ML}^{-1}\text{T}^{-2}\text{K}^{-1}$ ],  $\theta_n$  and  $\theta_o$  are fraction of solid phase and organic phase [-], respectively;  $T[\text{K}]$  is temperature;  $\lambda_{xz}(\theta)[\text{MLT}^{-3}\text{K}^{-1}]$  is apparent thermal

conductivity:

$$\lambda_{xz}(\theta) = \lambda_x C_w |q| \delta_{xz} + (\lambda_z - \lambda_x) C_w \frac{q_x q_z}{|q|} + \lambda_0(\theta) \delta_{xz}, \quad (16)$$

where  $\lambda_x$  and  $\lambda_z$  are components of thermal dispersivity in the horizontal and vertical directions [L];  $q$  [LT<sup>-1</sup>] is fluid flux density with its absolute value  $|q|$ , components in the horizontal and vertical directions,  $q_x$  and  $q_z$ , respectively;  $\delta_{xz}$  is Kronecker delta function;  $\lambda_0(\theta) = b_1 + b_2 \theta + b_3 \theta^{0.5}$  is thermal conductivity of soil in the absence of flow, where  $b_1$ ,  $b_2$  and  $b_3$  are empirical parameters, [MLT<sup>-3</sup>K<sup>-1</sup>]. In this example, the total simulation time is 10 hours. For more details about the model descriptions, one can refer to [Nakhaei and Šimůnek, 2014].

[Table 1]

Here the unknown model parameters are  $\alpha$ ,  $n$ ,  $K_s$ ,  $b_1$ ,  $b_2$  and  $b_3$ , which are assumed to be homogeneous in the domain and fit multivariate uniform prior distribution (Table 1). While other parameters are assumed to be known as listed in Table 2. To infer the 6 unknown model parameters, we collect pressure head and temperature measurements at  $t = 1, 2, \dots, 10$  hour at 3 locations denoted by the magenta circles in Figure 1.

[Table 2]

In this example, the high and low-fidelity models are constructed with different levels of discretization. In  $f_H(\mathbf{m})$ , the flow domain is evenly discretized into  $41 \times 41$  nodes. While in  $f_L(\mathbf{m})$ , there are  $21 \times 21$  nodes. In a Dell Precision T7610 workstation (Intel Xeon Processor E5-2680 v2 @ 2.80GHz; 512GB RAM; Windows 10 Pro., 64 Bit), the average time of evaluating  $f_H(\mathbf{m})$  is about 54 seconds, while the

average time of evaluating  $f_L(\mathbf{m})$  is about 6 seconds. As shown in Figure 2, although  $f_L(\mathbf{m})$  can capture the main trend of  $f_H(\mathbf{m})$ , systematic errors exist.

[Figure 2]

We first run MCMC with  $f_H(\mathbf{m})$  and  $f_L(\mathbf{m})$  respectively to approximate the posterior. Here the two MCMC simulations have 3 parallel chains with 5000 iterations, which means 15,000 model evaluations in total. As shown in Figure 3, the  $f_H(\mathbf{m})$ -based MCMC simulation can identify the unknown parameters properly, while the estimation results of the  $f_L(\mathbf{m})$ -based MCMC simulation are significantly biased, especially for the first three parameters. Thus, although using a low-fidelity model in the MCMC simulation can gain computational efficiency, the estimation accuracy cannot be guaranteed.

[Figure 3]

Then we run the AMF-MCMC algorithm with the same set of measurements to approximate the posterior. Here the initial number of  $f_L(\mathbf{m})$  evaluations is  $N_L = 300$ , and the initial number of  $f_H(\mathbf{m})$  evaluations is  $N_H = 30$ . Conditioned on these multi-fidelity data, we build the initial GP system,  $\tilde{g}_0(\mathbf{m})$ , based on which we can implement the MCMC simulation (3 parallel chains with 5000 iterations) very quickly. From the approximated posterior  $\tilde{p}_0(\mathbf{m}|\mathbf{d})$  we can draw a random parameter sample  $\mathbf{m}_{ap}$ , which is expected to be much closer to the posterior region than the  $N_H$  prior samples. We can add  $[\mathbf{m}_{ap} \ f_H(\mathbf{m}_{ap})]$  to the pool of  $f_H(\mathbf{m})$  evaluations to refine the GP system locally. Then the coupled process of GP-based MCMC simulation and GP refinement is further repeated 69 times.

[Figure 4]

As shown in Figure 4, the successively added new parameter samples (blue dots) for  $f_H(\mathbf{m})$  evaluations gradually approach to the true values (black crosses), which are the basis of a locally accurate GP system. Finally, we can obtain a rather accurate approximation of  $p(\mathbf{m}|\mathbf{d})$ . As shown in Figure 5, the marginal posterior probability density functions (PPDFs) obtained by the  $f_H(\mathbf{m})$ -MCMC algorithm and the AMF-MCMC algorithm are almost identical, which indicates the accuracy of the AMF-MCMC algorithm.

[Figure 5]

In the AMF-MCMC algorithm, the total numbers of  $f_H(\mathbf{m})$  and  $f_L(\mathbf{m})$  evaluations are 100 and 300, respectively. With respect to the number of model evaluations, the AMF-MCMC algorithm is much more efficient than both the  $f_H(\mathbf{m})$  and  $f_L(\mathbf{m})$ -based MCMC simulations. Nevertheless, the time needed by the multi-fidelity GP system constructions and GP-based MCMC simulations should not be neglected, especially when the number of model outputs  $N_d$  is large (we actually build  $N_d$  GPs for the  $N_d$  model outputs separately). To improve the efficiency of the AMF-MCMC algorithm, we can build the  $N_d$  GPs in parallel. In our simulations, there are 20 cores available, which can be utilized to greatly accelerate the simulation of the AMF-MCMC algorithm.

### 3.2. Example 2: Contaminant source identification with multimodal posterior

In example 2, we further test the performance of the AMF-MCMC algorithm in solving an inverse problem with multimodal posterior distribution. Here we consider

the processes of steady-state saturated groundwater flow and contaminant transport. As shown in Figure 6, the flow domain is  $20[\text{L}] \times 10[\text{L}]$ . The upper and lower sides are no-flow boundaries, the left ( $h = 12[\text{L}]$ ) and right ( $h = 11[\text{L}]$ ) sides are constant-head boundaries, respectively. At the initial time, hydraulic heads in the domain are all  $11[\text{L}]$  except for the left boundary ( $12[\text{L}]$ ).

[Figure 6]

Given the above initial and boundary conditions, we can obtain the flow field through numerically solving the following governing equations with MODFLOW [Harbaugh *et al.*, 2000]:

$$\frac{\partial}{\partial x_i} \left( K_i \frac{\partial h}{\partial x_i} \right) = 0, \quad (17)$$

and

$$v_i = -\frac{K_i}{\theta} \frac{\partial h}{\partial x_i}, \quad (18)$$

where  $x_i[\text{L}]$ ,  $K_i[\text{LT}^{-1}]$  and  $v_i[\text{LT}^{-1}]$  signify distance, hydraulic conductivity and pore water velocity along the respective Cartesian coordinate axis ( $i = 1, 2$ );  $h[\text{L}]$  is hydraulic head;  $\theta[-]$  is porosity of the aquifer. Here  $K = 8[\text{LT}^{-1}]$  and  $\theta = 0.25$  are known beforehand. In the steady-state flow field, some amount of contaminant is released from a point source located somewhere in the red dashed rectangle depicted in Figure 6. The contaminant source is characterized by 5 parameters, i.e., location,  $(x_s, y_s)[\text{L}]$ , source strength measured by mass loading rate,  $S_s[\text{MT}^{-1}]$ , start time of contaminant release,  $t_{\text{on}}[\text{T}]$ , and end time of the release,  $t_{\text{off}}[\text{T}]$ . Then we can obtain contaminant concentration  $C[\text{ML}^{-3}]$  at different times and locations through numerically solving the following advection-dispersion equation with MT3DMS

[Zheng and Wang, 1999]:

$$\frac{\partial(\theta C)}{\partial t} = \frac{\partial}{\partial x_i} \left( \theta D_{ij} \frac{\partial C}{\partial x_j} \right) - \frac{\partial}{\partial x_i} (\theta v_i C) + q_s C_s, \quad (19)$$

where  $t[\text{T}]$  is time;  $q_s[\text{T}^{-1}]$  and  $C_s[\text{ML}^{-3}]$  are volumetric flow rate per unit volume of the aquifer and concentration of the source, respectively;  $D_{ij}[\text{L}^2\text{T}^{-1}]$  are hydrodynamic dispersion coefficient tensors:

$$\begin{cases} D_{11} = (\alpha_L v_1^2 + \alpha_T v_2^2)/|v|, \\ D_{22} = (\alpha_L v_2^2 + \alpha_T v_1^2)/|v|, \\ D_{12} = D_{21} = (\alpha_L - \alpha_T)v_1 v_2/|v|, \end{cases} \quad (20)$$

where  $\alpha_L = 0.3[\text{L}^2\text{T}^{-1}]$  is the longitudinal dispersivity,  $\alpha_T = 0.03[\text{L}^2\text{T}^{-1}]$  is the transverse dispersivity, and  $|v| = \sqrt{v_1^2 + v_2^2}$  is the magnitude of the velocity.

In this example, the unknown parameters to be estimated are the 5 contaminant source parameters. Here we assume that our prior knowledge about them are rather limited and thus represented by a multivariate uniform distribution (Table 3). To infer the 5 unknown parameters, we collect concentration measurements at  $t = [6, 8, 10, 12, 14][\text{T}]$  at a well denoted by the blue circle in Figure 6. The measurements are generated with one set of true model parameters as shown in Table 3 with additive measurement errors that fit  $\mathcal{N}(0, 0.01^2)$ .

[Table 3]

In this example, the high-fidelity model  $f_H(\mathbf{m})$  is the coupled numerical model built with MODFLOW and MT3DMS. While the low-fidelity model  $f_L(\mathbf{m})$  is built with a data-driven surrogate, i.e., the adaptive sparse grid interpolation method proposed by Klimke and Wohlmuth [2005], based on 41 evaluations of  $f_H(\mathbf{m})$ . We compare the simulation results between  $f_H(\mathbf{m})$  and  $f_L(\mathbf{m})$  with 50 random

parameter samples drawn from the prior distribution and obtain  $R^2 = 0.949$  and  $RMSE = 0.167$ . It is noted here that we can also use other low-fidelity models, e.g., a numerical model with a coarser discretization. As data-driven surrogates are widely used in hydrologic science [Asher *et al.*, 2015; Razavi *et al.*, 2012], and many times in MCMC simulations [Elsheikh *et al.*, 2014; Laloy *et al.*, 2013; Zeng *et al.*, 2016], here we test the applicability in this example. Then we run MCMC with  $f_H(\mathbf{m})$  and  $f_L(\mathbf{m})$  respectively to approximate the posterior (6 parallel chains and 3000 iterations). As shown in Figure 7, the results obtained by the  $f_L(\mathbf{m})$ -based MCMC simulation are significantly biased, especially for  $x_s$  and  $t_{\text{off}}$ .

[Figure 7]

With the same set of measurements, we further run the AMF-MCMC algorithm to approximate the posterior. Here the initial number of  $f_L(\mathbf{m})$  evaluations is  $N_L = 300$ , and the initial number of  $f_H(\mathbf{m})$  evaluations is  $N_H = 30$ . Then we successively add another  $I_{\text{max}} = 50$  parameter samples for  $f_L(\mathbf{m})$  evaluations to refine the GP system over the posterior distribution. Finally, we can obtain a rather accurate approximation of  $p(\mathbf{m}|\mathbf{d})$ . As shown in Figure 8, the bivariate scatter plots obtained by the  $f_H(\mathbf{m})$ -MCMC algorithm and the AMF-MCMC algorithm are almost identical, which indicates the accuracy of the AMF-MCMC algorithm. Moreover, the bimodality of  $y_s$  is well identified by both algorithms.

[Figure 8]

#### 4. Conclusions and discussions

In this paper, we propose an efficient method for posterior exploration of hydrologic systems, i.e., the adaptive multi-fidelity simulation-based MCMC (AMF-MCMC) algorithm. In the AMF-MCMC algorithm, data from both a high-fidelity model and a low-fidelity model are fused to build a multi-fidelity GP system, based on which the MCMC simulation can be done quickly. As the region of our concern is the posterior distribution, we successively add new parameter samples that are close to this region for the high-fidelity model evaluation, which are used to refine the GP system locally. Finally, we can obtain an accurate estimation of the posterior distribution with very few evaluations of the high-fidelity model.

To demonstrate the performance of the AMF-MCMC algorithm, we test two numerical cases in inverse modeling of hydrologic systems. In the first example, we estimate soil hydraulic and thermal parameters with the proposed method in a single ring infiltration experiment. Here the low-fidelity model is built with HYDRUS-2D with a coarser discretization. In the second example, we test a contaminant source identification problem that has multimodal posterior. Here the low-fidelity model is built with a data-driven surrogate. In the two examples, the AMF-MCMC algorithm can obtain almost identical results as the high-fidelity model-based MCMC algorithm but with very low computational cost.

In the AMF-MCMC algorithm proposed in this paper, we only utilize data from two levels of model fidelity. If  $s$ -levels of data  $(\mathbf{D}_t(\mathbf{M}))_{t=1}^s$  sorted by increasing fidelity are available, we can readily extend the auto-regressive scheme:

$$u_t(\mathbf{m}) = \rho_{t-1} u_{t-1}(\mathbf{m}) + \delta_t(\mathbf{m}), t = 2, \dots, s, \quad (21)$$

where  $\delta_t(\mathbf{m})$  is a Gaussian process independent of  $\{u_{t-1}(\mathbf{m}), \dots, u_1(\mathbf{m})\}$ ,  $\rho_{t-1}$  is the cross-correlation coefficient. Moreover, we can consider complex, nonlinear relationship between  $u_{t-1}(\mathbf{m})$  and  $u_t(\mathbf{m})$  [Perdikaris *et al.*, 2017]:

$$u_t(\mathbf{m}) = q_{t-1}(u_{t-1}(\mathbf{m})) + \delta_t(\mathbf{m}), t = 2, \dots, s, \quad (22)$$

where  $q_{t-1}(\cdot)$  is nonlinear mapping. For the sake of clarity, these issues are not addressed in the present work. Furthermore, the multi-fidelity scheme can be straightforwardly combined with other inverse or data assimilation methods, e.g., iterative forms of ensemble smoother [Chen and Oliver, 2012; Emerick and Reynolds, 2013].

# Acknowledgments

Computer codes and data used are available upon request to the corresponding author.

The authors would like to thank Andreas Klimke from University of Stuttgart for providing sparse grid interpolation toolbox, Maziar Raissi from Brown University for providing MATLAB codes of multi-fidelity GP, respectively.

This work is supported by the National Natural Science Foundation of China (Grants 41371237 and 41271470).

# References

Anderson, M. P., W. W. Woessner, and R. J. Hunt (2015), *Applied groundwater modeling: simulation of flow and advective transport*, Academic press, San Diego, Calif. [Available

Asher, M. J., B. F. W. Croke, A. J. Jakeman, and L. J. M. Peeters (2015), A review of surrogate models and their application to groundwater modeling, *Water Resour. Res.*, 51(8), 5957-5973, doi: 10.1002/2015WR016967.

Chen, Y., and D. S. Oliver (2012), Ensemble Randomized Maximum Likelihood Method as an Iterative Ensemble Smoother, *Math. Geosci.*, 44(1), 1-26, doi: 10.1007/s11004-011-9376-z.

Clark, M. P., D. Kavetski, and F. Fenicia (2011), Pursuing the method of multiple working hypotheses for hydrological modeling, *Water Resour. Res.*, 47(9), W09301, doi: 10.1029/2010WR009827.

Efendiev, Y., A. Datta-Gupta, V. Ginting, X. Ma, and B. Mallick (2005), An efficient two-stage Markov chain Monte Carlo method for dynamic data integration, *Water Resour. Res.*, 41(12), W12423, doi: 10.1029/2004wr003764.

Elsheikh, A. H., I. Hoteit, and M. F. Wheeler (2014), Efficient Bayesian inference of subsurface flow models using nested sampling and sparse polynomial chaos surrogates, *Comput. Method Appl. M.*, 269, 515-537, doi: 10.1016/j.cma.2013.11.001.

Emerick, A. A., and A. C. Reynolds (2013), Ensemble smoother with multiple data assimilation, *Comput. Geosci.*, 55, 3-15, doi: 10.1016/j.cageo.2012.03.011.

Gong, W., and Q. Duan (2017), An adaptive surrogate modeling-based sampling strategy for parameter optimization and distribution estimation (ASMO-PODE), *Environ. Modell. Softw.*, 95, 61-75, doi: 10.1016/j.envsoft.2017.05.005.

Haario, H., M. Laine, A. Mira, and E. Saksman (2006), DRAM: efficient adaptive MCMC, *Stat. Comput.*, 16(4), 339-354, doi: 10.1007/s11222-006-9438-0.

Harbaugh, A. W., E. R. Banta, M. C. Hill, and M. G. McDonald (2000), MODFLOW-2000, The US Geological Survey Modular Ground-Water Model: User Guide to Modularization Concepts and the Ground-Water Flow Process, U.S. Geol. Surv., Reston, Va. [Available at <https://pubs.usgs.gov/of/2000/0092/report.pdf>.]

Kennedy, M. C., and A. O'Hagan (2000), Predicting the output from a complex computer code when fast approximations are available, *Biometrika*, 87(1), 1-13, doi: DOI 10.1093/biomet/87.1.1.

Klimke, A., and B. Wohlmuth (2005), Algorithm 847: spinterp: Piecewise multilinear hierarchical sparse grid interpolation in MATLAB, *ACM T. Math. Software*, 31(4), 561-579, doi: Doi 10.1145/1114268.1114275.

Laloy, E., B. Rogiers, J. A. Vrugt, D. Mallants, and D. Jacques (2013), Efficient posterior exploration of a high-dimensional groundwater model from two-stage Markov chain Monte Carlo simulation and polynomial chaos expansion, *Water Resour. Res.*, 49(5), 2664-2682, doi: 10.1002/wrcr.20226.

Le Gratiet, L., and J. Garnier (2014), Recursive co-Kriging model for design of computer experiments with multiple levels of fidelity, *Int. J. Uncertain. Quan.*, 4(5), 365-386, doi: 10.1615/Int.J.UncertaintyQuantification.2014006914.

Mualem, Y. (1976), A new model for predicting the hydraulic conductivity of unsaturated porous media, *Water Resour. Res.*, 12(3), 513-522, doi: 10.1029/WR012i003p00513.

Nakhaei, M., and J. Šimůnek (2014), Parameter estimation of soil hydraulic and thermal property functions for unsaturated porous media using the HYDRUS-2D code, *J. Hydrol. Hydromech.*, 62(1), 7-15, doi: 10.2478/johh-2014-0008.

Narayan, A., C. Gittelson, and D. Xiu (2014), A stochastic collocation algorithm with multifidelity models,

*SIAM J. Sci. Comput.*, 36(2), A495-A521, doi: 10.1137/130929461.

Palar, P. S., T. Tsuchiya, and G. T. Parks (2016), Multi-fidelity non-intrusive polynomial chaos based on regression, *Comput. Method. Appl. M.*, 305, 579-606, doi: 10.1016/j.cma.2016.03.022.

Parussini, L., D. Venturi, P. Perdikaris, and G. E. Karniadakis (2017), Multi-fidelity Gaussian process regression for prediction of random fields, *J. Comput. Phys.*, 336, 36-50, doi: 10.1016/j.jcp.2017.01.047.

Perdikaris, P., M. Raissi, A. Damianou, N. Lawrence, and G. E. Karniadakis (2017), Nonlinear information fusion algorithms for data-efficient multi-fidelity modelling, *Proc. R. Soc. A*, 473, 20160751, doi: 10.1098/rspa.2016.0751.

Raissi, M., P. Perdikaris, and G. E. Karniadakis (2017), Inferring solutions of differential equations using noisy multi-fidelity data, *J. Comput. Phys.*, 335, 736-746, doi: 10.1016/j.jcp.2017.01.060.

Razavi, S., B. A. Tolson, and D. H. Burn (2012), Review of surrogate modeling in water resources, *Water Resour. Res.*, 48, W07401, doi: 10.1029/2011WR011527.

Refsgaard, J. C., S. Christensen, T. O. Sonnenborg, D. Seifert, A. L. Højberg, and L. Troldborg (2012), Review of strategies for handling geological uncertainty in groundwater flow and transport modeling, *Adv. Water Resour.*, 36, 36-50, doi: 10.1016/j.advwatres.2011.04.006.

Šimůnek, J., M. T. van Genuchten, and M. Šejna (2008), Development and applications of the HYDRUS and STANMOD software packages and related codes, *Vadose Zone J.*, 7(2), 587-600, doi: 10.2136/vzj2007.0077.

Smith, R. C. (2014), *Uncertainty Quantification: Theory, Implementation, and Applications*, SIAM, Philadelphia, Pa. [Available

Smith, T. J., and L. A. Marshall (2008), Bayesian methods in hydrologic modeling: A study of recent advancements in Markov chain Monte Carlo techniques, *Water Resour. Res.*, 44(12), W00B05, doi: 10.1029/2007WR006705.

Sophocleous, M. (1979), Analysis of water and heat-flow in unsaturated-saturated porous media, *Water Resour. Res.*, 15(5), 1195-1206, doi: 10.1029/WR015i005p01195.

Stuart, A. M. (2010), Inverse problems: A Bayesian perspective, *Acta Numer.*, 19, 451-559, doi: 10.1017/S0962492910000061.

Vangenuchten, M. T. (1980), A closed-form equation for predicting the hydraulic conductivity of unsaturated soils, *Soil. Sci. Soc. Am. J.*, 44(5), 892-898, doi: 10.2136/sssaj1980.03615995004400050002x.

Vieux, B. E. (2001), Distributed hydrologic modeling using GIS, in *Water Science and Technology Library*, vol 38, Springer, Dordrecht.

Vrugt, J. A. (2016), Markov chain Monte Carlo simulation using the DREAM software package: Theory, concepts, and MATLAB implementation, *Environ. Modell. Softw.*, 75, 273-316, doi: 10.1016/j.envsoft.2015.08.013.

Vrugt, J. A., C. J. F. ter Braak, M. P. Clark, J. M. Hyman, and B. A. Robinson (2008), Treatment of input uncertainty in hydrologic modeling: Doing hydrology backward with Markov chain Monte Carlo simulation, *Water Resour. Res.*, 44(12), W00B09, doi: 10.1029/2007WR006720.

Vrugt, J. A., C. J. F. ter Braak, C. G. H. Diks, B. A. Robinson, J. M. Hyman, and D. Higdon (2009), Accelerating Markov Chain Monte Carlo Simulation by Differential Evolution with Self-Adaptive Randomized Subspace Sampling, *Int. J. Nonlin. Sci. Num.*, 10(3), 273-290, doi: 10.1515/IJNSNS.2009.10.3.273.

Wagener, T., and H. V. Gupta (2005), Model identification for hydrological forecasting under uncertainty, *Stoch. Environ. Res. Risk Assess.*, 19(6), 378-387, doi: 10.1007/s00477-005-0006-5.

Williams, C. K., and C. E. Rasmussen (2006), *Gaussian Processes for Machine Learning*, MIT Press, Cambridge, Mass. [Available at <http://www.gaussianprocess.org/gpml/chapters/>.]

Zeng, L., L. Shi, D. Zhang, and L. Wu (2012), A sparse grid based Bayesian method for contaminant source identification, *Adv. Water Resour.*, 37, 1-9, doi: 10.1016/j.advwatres.2011.09.011.

Zeng, X. K., M. Ye, J. Burkardt, J. C. Wu, D. Wang, and X. B. Zhu (2016), Evaluating two sparse grid surrogates and two adaptation criteria for groundwater Bayesian uncertainty quantification, *J. Hydrol.*, 535, 120-134, doi: 10.1016/j.jhydrol.2016.01.058.

Zhang, J., W. Li, L. Zeng, and L. Wu (2016), An adaptive Gaussian process-based method for efficient Bayesian experimental design in groundwater contaminant source identification problems, *Water Resour. Res.*, 52(8), 5971-5984, doi: 10.1002/2016WR018598.

Zhang, J., L. Zeng, C. Chen, D. Chen, and L. Wu (2015), Efficient Bayesian experimental design for contaminant source identification, *Water Resour. Res.*, 51(1), 576-598, doi: 10.1002/2014WR015740.

Zheng, C., and P. P. Wang (1999), MT3DMS: A modular three-dimensional multispecies transport model for simulation of advection, dispersion, and chemical reactions of contaminants in groundwater systems; documentation and user's guide, *Contract Rep. SERDP-99-1*, U.S. Army Eng. Res. and Dev. Cent., Vicksburg, Miss. [Available at <http://www.geology.wisc.edu/courses/g727/mt3dmanual.pdf>.]

Zhu, X., A. Narayan, and D. Xiu (2014), Computational aspects of stochastic collocation with multifidelity models, *SIAM-ASA J. Uncertain.*, 2(1), 444-463, doi: 10.1137/130949154.

# Tables

Table 1 Prior ranges and true values of unknown model parameters in the first example

Parameters	Prior ranges	True values
$\alpha[\text{cm}^{-1}]$	[0.0190 0.0930]	0.0387
$n[-]$	[1.360 2.370]	2.210
$K_s[\text{cm h}^{-1}]$	[4.828 11.404]	6.759
$b_1[\text{kg cm h}^{-3} \text{K}^{-1}]$	$[2.179 \times 10^{12} \ 4.857 \times 10^{12}]$	$2.948 \times 10^{12}$
$b_2[\text{kg cm h}^{-3} \text{K}^{-1}]$	$[4.778 \times 10^{11} \ 2.426 \times 10^{12}]$	$2.118 \times 10^{12}$
$b_3[\text{kg cm h}^{-3} \text{K}^{-1}]$	$[2.174 \times 10^{12} \ 5.184 \times 10^{12}]$	$2.972 \times 10^{12}$

Table 2 Values of known model parameters in the first example

Parameters	Values	Parameters	Values
$\theta_r[-]$	0.041	$l[-]$	0.500
$\theta_s[-]$	0.430	$C_w[\text{J cm}^{-3} \text{K}^{-1}]$	4.180
$\theta_n[-]$	0.600	$C_n[\text{J cm}^{-3} \text{K}^{-1}]$	1.920
$\theta_o[-]$	0.001	$C_o[\text{J cm}^{-3} \text{K}^{-1}]$	2.510
$\lambda_x[\text{cm}]$	0.200	$\lambda_y[\text{cm}]$	2.000

Table 3 Prior ranges and true values of unknown model parameters in the second example

Parameters	$x_s[\text{L}]$	$y_s[\text{L}]$	$S_s[\text{MT}^{-1}]$	$t_{\text{on}}[\text{T}]$	$t_{\text{off}}[\text{T}]$
Ranges	[3 5]	[3 7]	[10 13]	[3 5]	[9 11]
True values	3.854	5.999	11.044	4.897	9.075

# Figures

Figure 1. Flow domain for the first example.

Figure 2. Comparison of (a) simulated head outputs, (b) simulated temperature outputs, between  $f_H(\mathbf{m})$  and  $f_L(\mathbf{m})$ .

Figure 3. Trace plots of model parameters obtained by the  $f_H(\mathbf{m})$ - MCMC algorithm (red dots) and the  $f_L(\mathbf{m})$ - MCMC algorithm (blue dots) in the first example. The true values are represented by the black crosses.

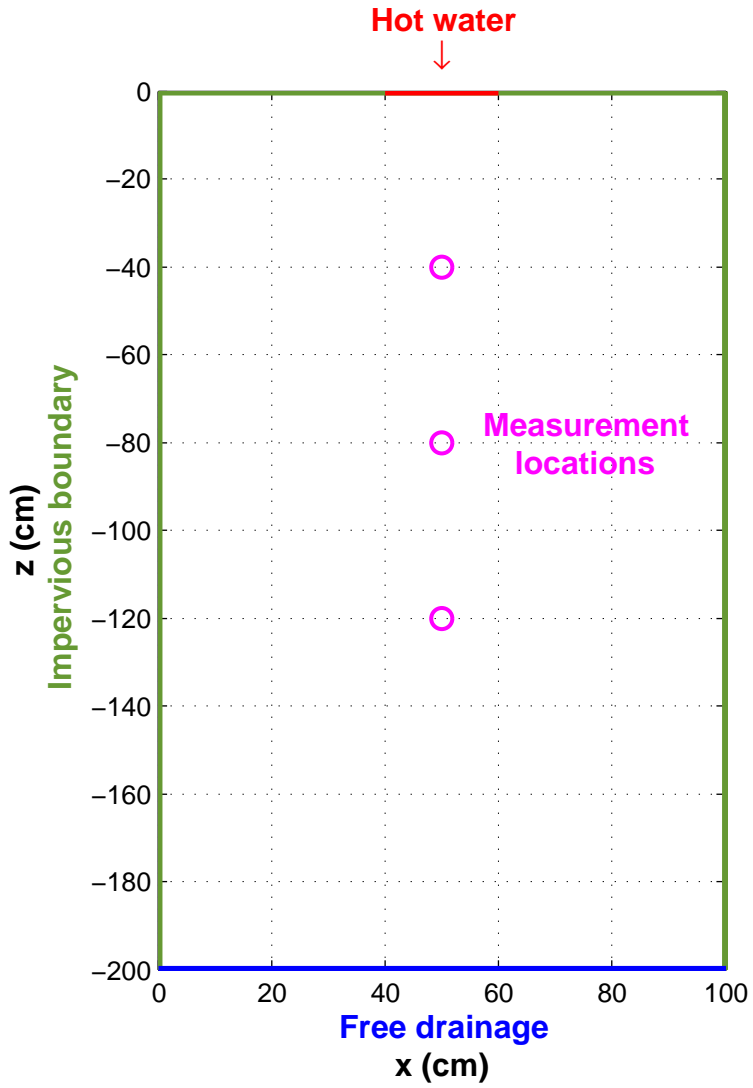
Figure 4.  $N_H$  initial parameter samples (red dots) and  $I_{\max}$  successively added parameter samples (blue dots) for  $f_H(\mathbf{m})$  evaluations. The true values are represented by the black crosses.

Figure 5. Marginal PPDFs obtained by the  $f_H(\mathbf{m})$ -MCMC algorithm (red curves) and the AMF-MCMC algorithm (blue dashed curves). The true values are represented by the vertical black lines.

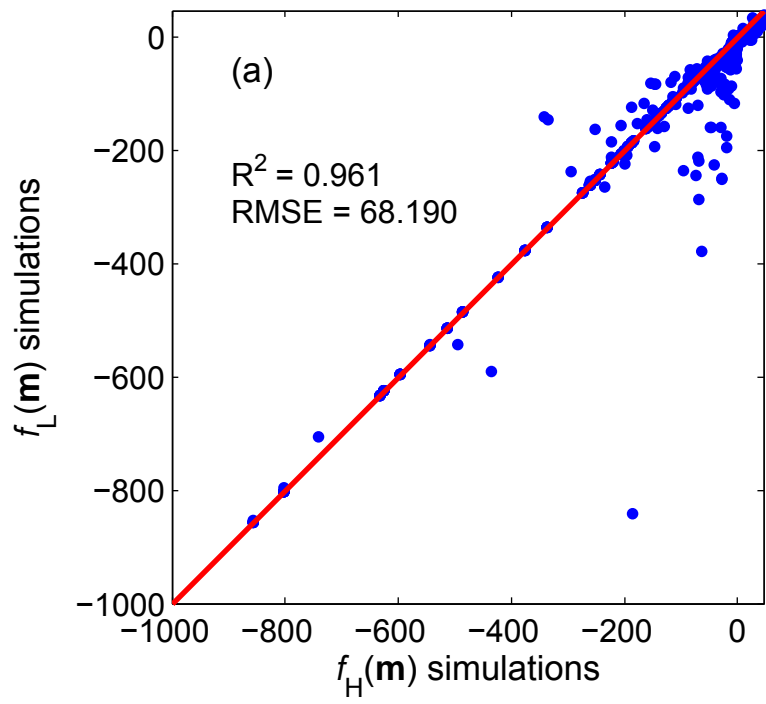
Figure 6. Flow domain for the second example.

Figure 7. Trace plots of model parameters obtained by the  $f_H(\mathbf{m})$ - MCMC algorithm (red dots) and the  $f_L(\mathbf{m})$ - MCMC algorithm (blue dots) in the second example. The true values are represented by the black crosses.

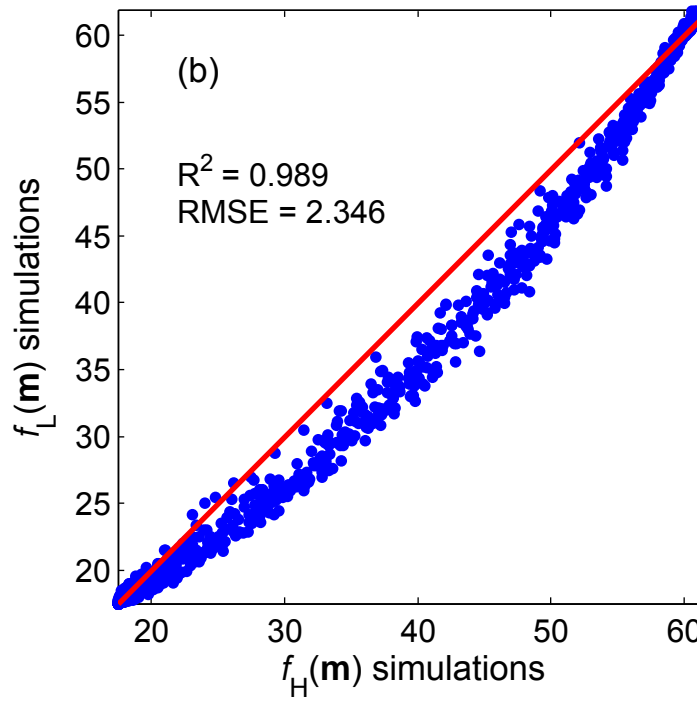
Figure 8. Bivariate scatter plots obtained by the  $f_H(\mathbf{m})$ -MCMC algorithm (red dots) and the AMF-MCMC algorithm (blue dots) in the second example. The true values are represented by the black crosses.

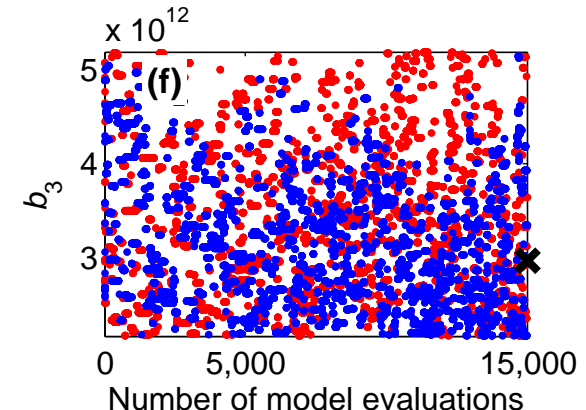
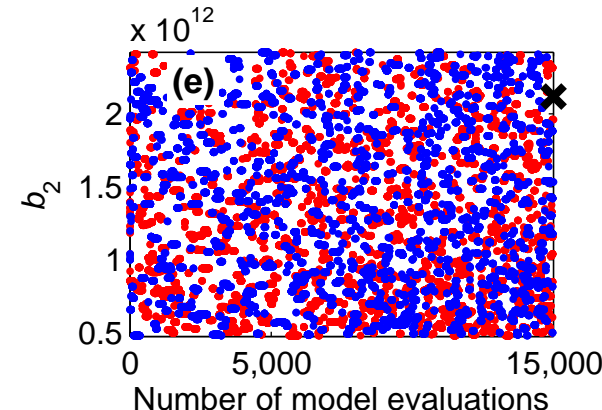
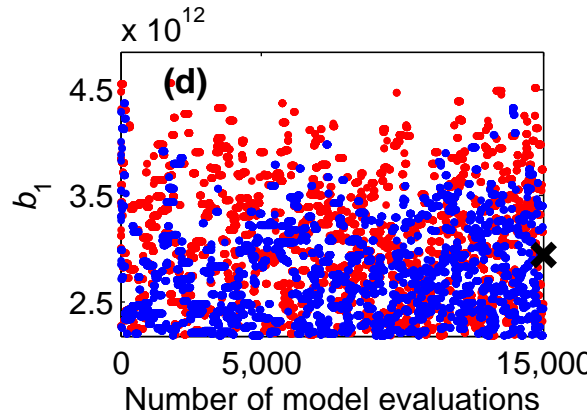
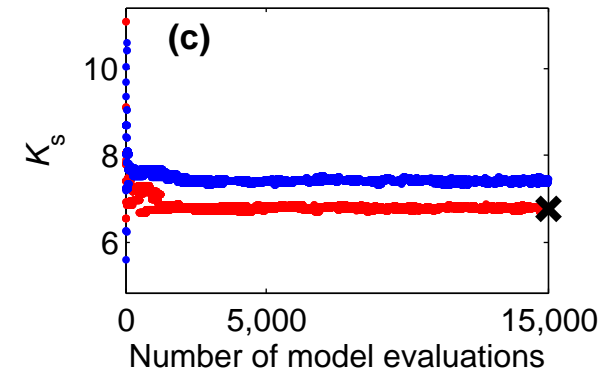
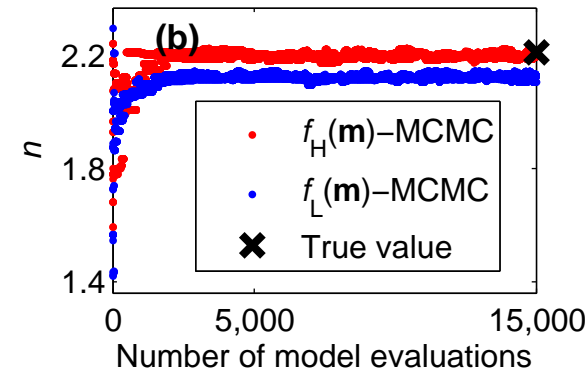
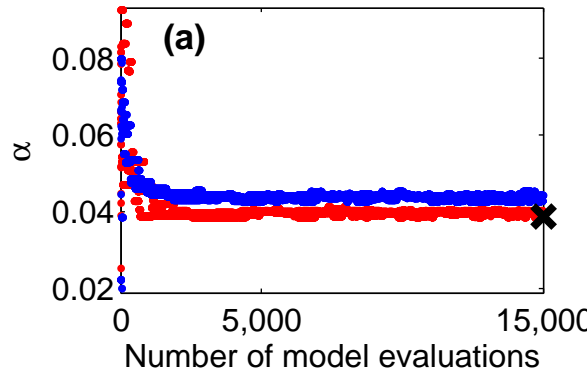


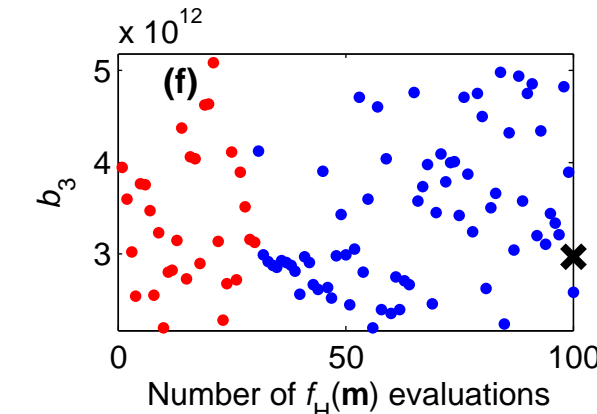
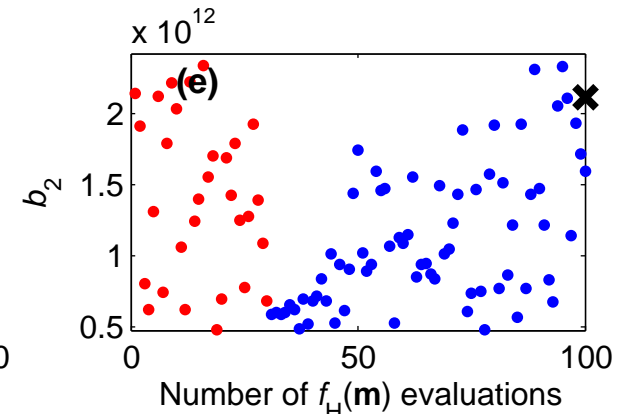
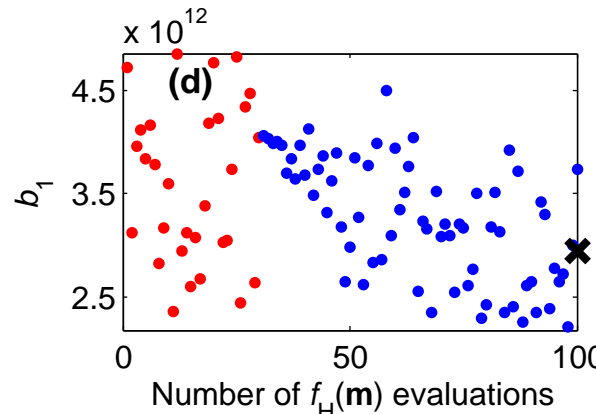
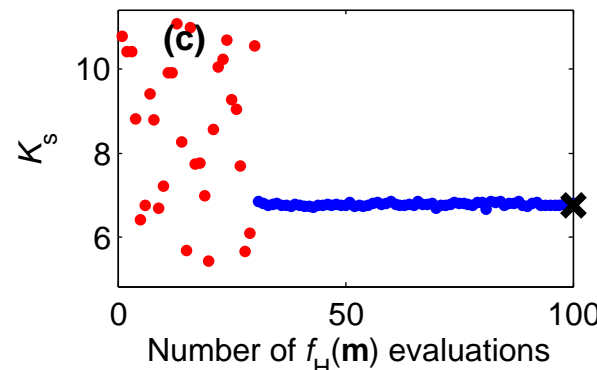
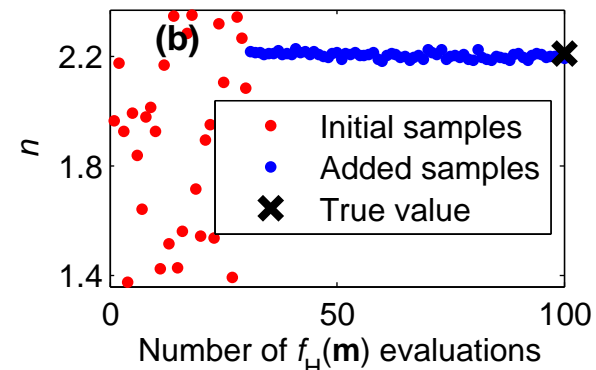
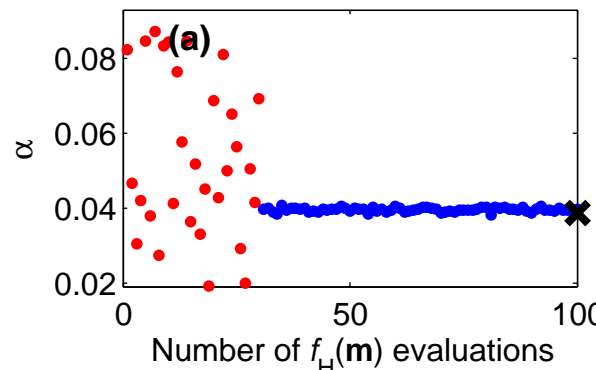
Head outputs

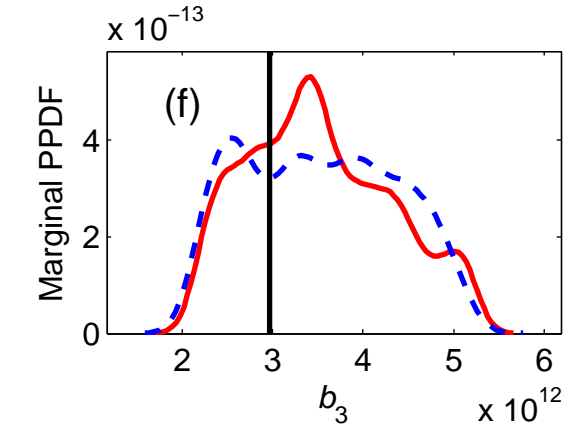
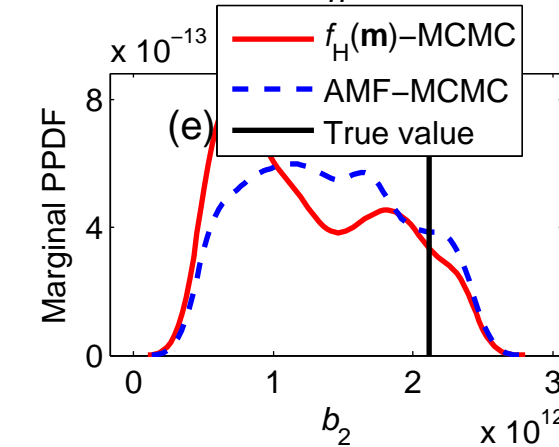
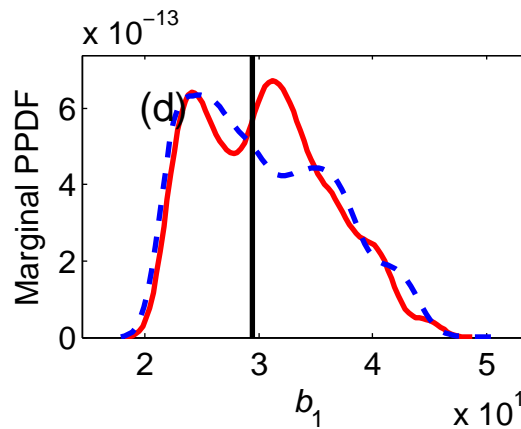
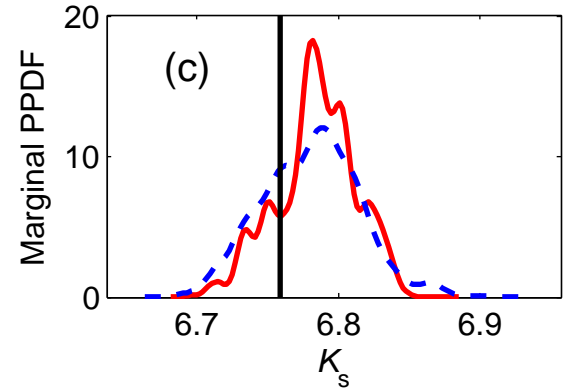
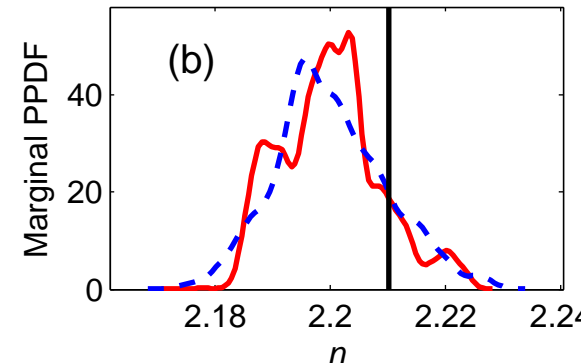
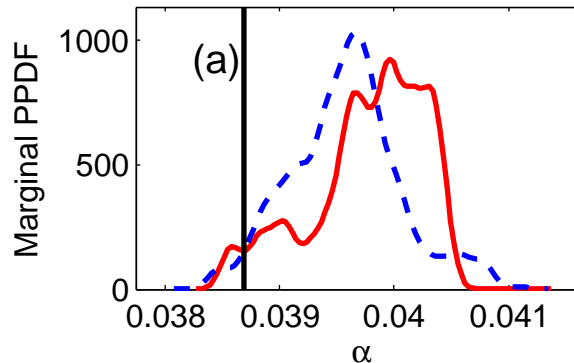


Temperature outputs









No flow

10 [L]

$h = 12$  [L]

S



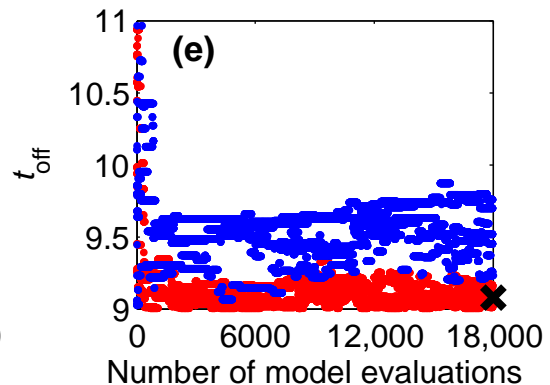
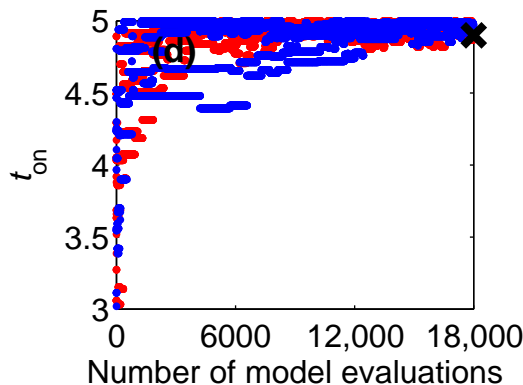
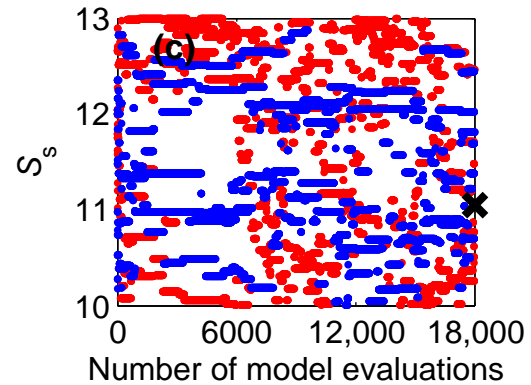
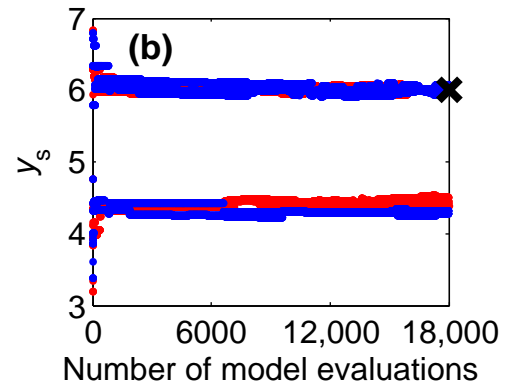
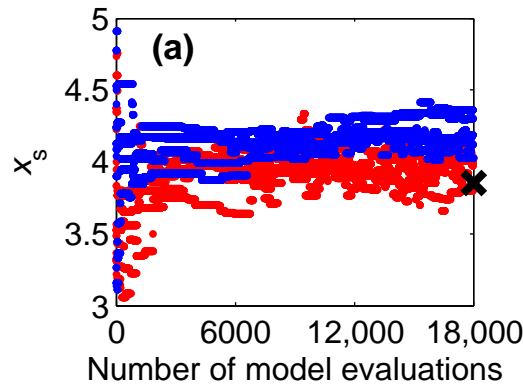
Measurement  
location

0

20 [L]

No flow

$h = 11$  [L]



- $f_H(m)$ -MCMC
- $f_L(m)$ -MCMC
- × True value

